Yamazaki, Y., Stolle, C., Matzka, J., Liu, H., Tao, C. (2018): Interannual Variability of the Daytime Equatorial Ionospheric Electric Field. - *Journal of Geophysical Research*, *123*, 5, pp. 4241—4256.

DOI: http://doi.org/10.1029/2017JA025165

Journal of Geophysical Research: Space Physics

RESEARCH ARTICLE
10.1029/2017JA025165

Interannual Variability of the Daytime Equatorial Ionospheric Electric Field

Yosuke Yamazaki[1], Claudia Stolle[1,2], Jürgen Matzka[1], Huixin Liu[3,4], and Chihiro Tao[5]

[1]GFZ German Research Centre for Geosciences, Potsdam, Germany, [2]Faculty of Science, University of Potsdam, Potsdam, Germany, [3]Department of Earth and Planetary Sciences, Kyushu University, Fukuoka, Japan, [4]International Center for Space Weather Research and Education, Kyushu University, Fukuoka, Japan, [5]National Institute of Information and Communications Technology, Tokyo, Japan

Key Points:
- Interannual variation of the equatorial electric field is examined
- GAIA model reproduces observations without variable magnetospheric forcing
- Lower-atmospheric forcing dominates the variability at 1200 LT

Correspondence to:
Y. Yamazaki,
yamazaki@gfz-potsdam.de

Citation:
Yamazaki, Y., Stolle, C., Matzka, J., Liu, H., & Tao, C. (2018). Interannual variability of the daytime equatorial ionospheric electric field. *Journal of Geophysical Research: Space Physics*, *123*, 4241–4256. https://doi.org/10.1029/2017JA025165

Received 27 DEC 2017
Accepted 24 APR 2018
Accepted article online 9 MAY 2018
Published online 19 MAY 2018

Abstract Understanding the variability of the ionosphere is important for the prediction of space weather and climate. Recent studies have shown that forcing from the lower atmosphere plays a significant role for the short-term (day-to-day) variability of the low-latitude ionosphere. The present study aims to assess the importance of atmospheric forcing for the variability of the daytime equatorial ionospheric electric field on the interannual (year-to-year) time scale. Magnetic field measurements from Huancayo (12.05°S, 75.33°W) are used to augment the equatorial vertical plasma drift velocity (V_Z) measurements from the Jicamarca Unattended Long-term Investigations of the Ionosphere and Atmosphere radar during 2001–2016. V_Z can be regarded as a measure of the zonal electric field. After removing the seasonal variation of ~10 m/s, midday values of V_Z show an interannual variation of ~2 m/s with an oscillation period of 2–3 years. No evidence of solar cycle influence is found. The Ground-to-topside Atmosphere-Ionosphere model for Aeronomy, which takes into account realistic atmospheric variability below 30 km, reproduces the pattern of the observed interannual variation without having to include variable forcing from the magnetosphere. The results indicate that lower atmospheric forcing plays a dominant role for the observed interannual variability of V_Z at 1200 local time.

1. Introduction

The zonal electric field in the equatorial ionosphere is typically on the order of 10^{-4} V/m (Alken et al., 2013; Balsley, 1973; Fejer, 1981; Richmond, 1995a). The electromotive force responsible for the equatorial electric field is generated by the dynamo action of neutral winds in the thermosphere (Du & Stening, 1999; Maute et al., 2012; Stening, 1995). The zonal electric field is closely associated with the vertical plasma motion over the magnetic equator, as the ionospheric plasma tends to move in the direction of $\mathbf{E} \times \mathbf{B}$ (e.g., Richmond, 1995b), where $\mathbf{E}$ is the electric field and $\mathbf{B}$ is the Earth's main magnetic field. (Note that $\mathbf{B}$ is completely horizontal at the magnetic equator.) Ground and satellite measurements of the equatorial vertical plasma velocity (V_Z) have revealed upward ($V_Z > 0$) and downward ($V_Z < 0$) drifts during daytime and nighttime, respectively, corresponding to the eastward and westward electric fields (Fejer et al., 1979, 2008; Kil et al., 2007; Scherliess & Fejer, 1999; Woodman, 1970). The daytime eastward electric field drives the equatorial electrojet, which is a narrow band of relatively strong *E* region current flow (several amperes per square kilometer) along the magnetic equator (Alken & Maus, 2007; Lühr et al., 2004).

In the daytime *F* region, the equatorial plasma, which is lifted by the upward drift, diffuses downward and poleward along geomagnetic field lines due to gravity and plasma pressure gradients (Hanson & Moffett, 1966). As a result, there is a depletion of the plasma density over the magnetic equator and a local plasma density maximum on both sides of the magnetic equator (about 15°–20° away from the magnetic equator). This plasma density structure in the daytime *F* region is referred to as the equatorial ionization anomaly (EIA) (e.g., Jee et al., 2004; Lin et al., 2007). Studies have shown that the intensity and location of the two EIA crests depend strongly on the equatorial electric field (Rastogi & Klobuchar, 1990; Rush & Richmond, 1973; Stolle et al., 2008). Therefore, understanding the behavior of the equatorial electric field is important for the prediction of the *F* region plasma distribution.

Traditionally, studies of the low-latitude ionosphere considered two types of external energy sources. One is solar radiation especially at extreme ultraviolet (EUV) and X-ray wavelengths, which are most significant

for the heating and photoionization of the upper atmosphere (e.g., Solomon & Qian, 2005). The solar activity cycle causes the 11-year variation of the plasma density (e.g., Li et al., 2018; Liu et al., 2007; Zhao et al., 2009) and currents (e.g., Matzka et al., 2017; Yamazaki et al., 2011) in the low-latitude ionosphere. The other external source of ionospheric variability is the energy deposition from the magnetosphere (e.g., Fuller-Rowell et al., 1994; Lu et al., 2014). Disturbances of the ionosphere start in the polar region but eventually extend to lower latitudes. Observations have shown that the equatorial ionosphere can be significantly disturbed during geomagnetic storms (e.g., Lin et al., 2005; Nava et al., 2016). Empirical models of the ionosphere often involve solar flux indices, such as $F_{10.7}$ (Tapping, 2013), and geomagnetic indices, such as *Kp*, to take into account the influence of solar and magnetospheric forcing, respectively (e.g., Bilitza et al., 2014; Lean et al., 2011; Mukhtarov, Andonov, et al., 2013; Mukhtarov, Pancheva, et al., 2013; Themens et al., 2017).

Studies in the last decade have revealed that the upper atmosphere is also under a significant influence of forcing from the lower layers of the atmosphere. The energy and momentum can be transferred from the lower atmosphere to the upper atmosphere in the form of various atmospheric waves (e.g., Liu, 2016a; Oberheide et al., 2015; Yiğit & Medvedev, 2015). Model studies have shown that lower-atmospheric forcing can make a significant contribution to the short-term (day-to-day) variability in the low-latitude ionosphere (Fang et al., 2013; Jin et al., 2011; Liu et al., 2013; Maute et al., 2016; Pedatella et al., 2016). Observations have also provided evidence to support the effect of lower-atmospheric forcing on the upper atmosphere. For example, significant disturbances were observed in the low-latitude ionosphere following the January 2009 sudden stratospheric warming event (e.g., Chau et al., 2010; Goncharenko, Chau, et al., 2010; Goncharenko, Coster, et al., 2010; Liu et al., 2011; Pedatella et al., 2014; Yamazaki et al., 2012; Yue et al., 2010). Such disturbances cannot be reproduced by traditional empirical models that consider only solar and magnetospheric forcing.

The present study also concentrates on the lower-atmospheric impact on the upper atmosphere, but our focus is on interannual variability, which has been much less explored. By interannual variability, we mean the changes that occur from 1 year to the next, or longer. In this study, we consider the time scales longer than a year up to a solar cycle (11 years). Recently, we reported on the interannual variability of the ionospheric solar quiet (S_q) current system (Yamazaki et al., 2017). We found an interannual variation with a period of approximately 28 months in the central position of the S_q current loop over Japan during 2005–2013, when solar and magnetospheric activities were relatively low. It was suspected that the 28-month variation of S_q might be caused by atmospheric tides in the dynamo region (90–150 km), which showed similar variability due to the influence of the quasi-biennial oscillation (QBO) (Baldwin et al., 2001) in the tropical stratosphere. Since the dynamo region winds lead to both S_q currents and ionospheric electric field, the interannual variation of the electric field might also contain useful information regarding the possible effect of lower-atmospheric forcing. In this study, we determine for the first time the interannual variability of the daytime equatorial electric field using measurements from the Peruvian sector. The results are compared with a first-principle model to evaluate the contribution of lower-atmospheric forcing.

2. Data and Model

2.1. JULIA radar

The Jicamarca Unattended Long-term Investigations of the Ionosphere and Atmosphere (JULIA) radar (Hysell et al., 1997) is located in the Jicamarca Radio Observatory (11.97°S, 76.87°W), near Lima, Peru (see Figure 1). The JULIA radar routinely measures the vertical Doppler velocity of the so-called "150-km echoes," which are typically observed in the height range of 140–170 km during daytime hours (Chau & Kudeki, 2006). This quantity is known to give a measure of the $\mathbf{E}\times\mathbf{B}$ vertical plasma drift velocity (V_Z) (Chau & Woodman, 2004; Kudeki & Fawcett, 1993), which is related to the zonal electric field. We used the average velocity over 140–170 km measured at 5-min intervals during August 200 to March 2016, which were obtained from the Madrigal database (jro.igp.gob.pe/madrigal/).

2.2. Magnetometers

We used ground-based magnetometer data from the Huancayo Geomagnetic Observatory (12.05°S, 75.33°W), located close to the Jicamarca Radio Observatory (see Figure 1). Being near the magnetic equator, the horizontal (*H*) component of the geomagnetic field at Huancayo shows large daily variations due to the equatorial electrojet. The 1-min resolution data were obtained from the World Data Center for Geomagnetism, Edinburgh (www.wdc.bgs.ac.uk) for 2001–2002 and from the INTERMAGNET (Love & Chulliat, 2013) (www.intermagnet.org) from 2003 onward.

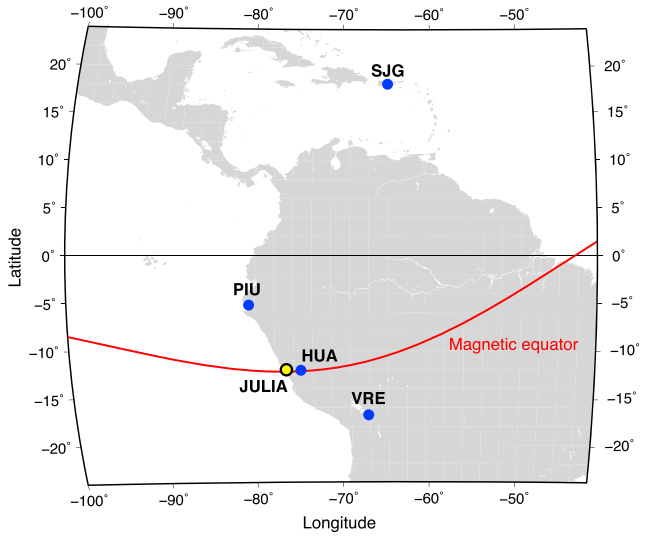

Figure 1. Map of stations in the American longitude sector used for this study. Blue dots indicate ground magnetometer stations, while the yellow dot shows the location of the Jicamarca Unattended Long-term Investigations of the Ionosphere and Atmosphere (JULIA) radar. The red line indicates the magnetic equator for January 2013. The Quasi-Dipole latitude is 0.18°N at Huancayo (HUA), 6.69°N at Piura (PIU), 5.20°S at Villa Remedios (VRE), and 26.58°N at San Juan (SJG), for January 2013. LT = local time.

We also used the 1-min data from the following stations: Villa Remedios (16.77°S, 68.17°W), Piura (5.17°S, 80.64°W), and San Juan (18.12°N, 66.15°W). These stations are all located in the American longitude sector outside the equatorial electrojet belt, which extends approximately ±3° from the magnetic equator. Thus, the influence of the equatorial electrojet is less than at Huancayo. The location of these stations is indicated in Figure 1. The 1-min data from Villa Remedios for January 2013 are available at GFZ Data Services (Matzka et al., 2018). The Piura data and the San Juan data can be obtained from the Low-Latitude Ionospheric Sensor Network (LISN) database (lisn.igp.gob.pe) and the INTERMAGNET, respectively.

2.3. GAIA Model

Ground-to-topside model of Atmosphere and Ionosphere for Aeronomy (GAIA) is a physics-based model of the coupled atmosphere-ionosphere system, extending from the ground to the exobase (e.g., Jin et al., 2011; Liu et al., 2013; Miyoshi et al., 2012). The horizontal resolution of the model is 2.8° in longitude and latitude, and the vertical resolution is a grid point per 0.2 scale height. GAIA incorporates an ionospheric wind dynamo model that enables the calculation of the equatorial vertical plasma drift velocity (Jin et al., 2008).

Miyoshi et al. (2017) performed a long-term GAIA simulation for the years 1997–2013. Later, the simulation was extended until 2016 (Liu et al., 2017; Yamazaki et al., 2017). The present study uses the model outputs from this long-term run. Following Jin et al. (2012), the lower atmosphere below 30 km was constrained with meteorological reanalysis data using a nudging technique. Specifically, 6-hourly data from the Japanese 25-year Reanalysis (Onogi et al., 2007) were used for 1997–2013 and the Japanese 55-year Reanalysis (Kobayashi et al., 2015) from 2014 onward. This procedure introduces realistic atmospheric variability in the lower atmosphere that acts as external forcing for the upper atmosphere, including the variability on the interannual time scale. The $F_{10.7}$ index was used as a proxy of the solar extreme ultraviolet flux intensity, which can also induce interannual variability. The cross polar cap potential, which relates to the energy deposition from the magnetosphere, was assumed to be low and constant (= 30 kV) throughout the simulation so that the interannual variability will not result from magnetospheric forcing.

3. Estimation of V_Z using Magnetometer Data

In this section, we explain how we derived monthly mean values of the midday V_Z using a combination of JULIA radar data and Huancayo magnetometer data. It was necessary to include the magnetometer data due to gaps in the temporal coverage of the JULIA radar measurements. The JULIA V_Z data cover approximately 140 days/year, and they are not evenly distributed throughout the year. This makes it sometimes difficult to derive a robust estimate of the monthly mean value of V_Z. Figure 2a shows the availability of JULIA V_Z data

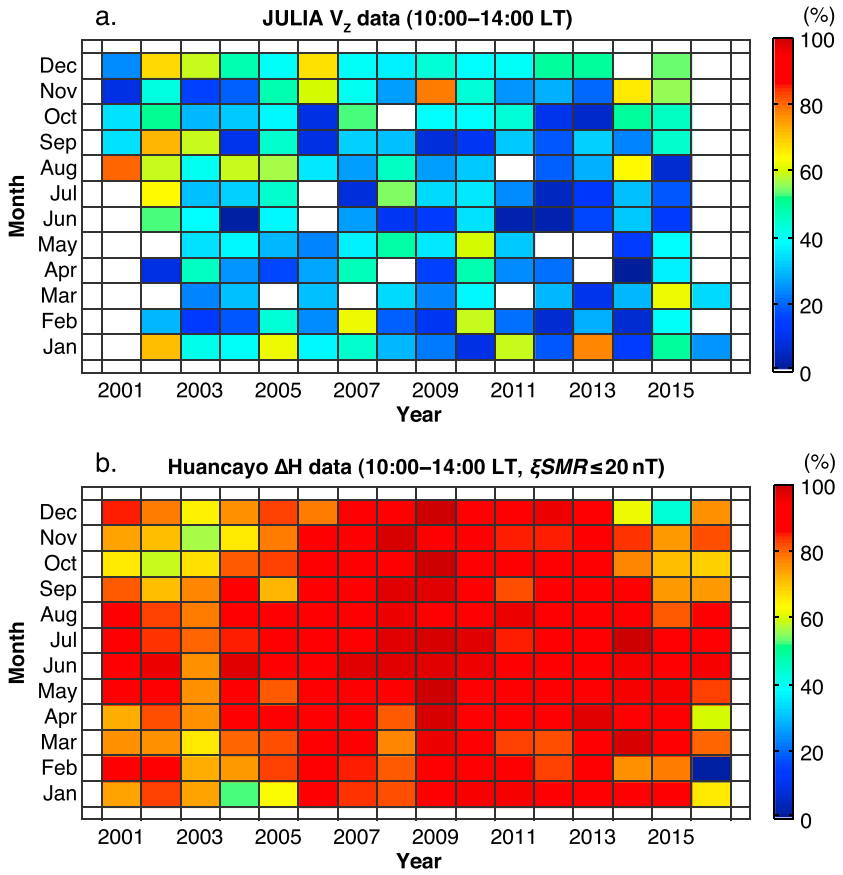

Figure 2. Availability of the daytime data (1000–1400 LT) for (a) the equatorial vertical plasma drift velocity V_Z from the Jicamarca Unattended Long-term Investigations of the Ionosphere and Atmosphere (JULIA) radar and (b) the geomagnetic field at Huancayo when ξSMR $\leq$ 20 nT. The parameter ξSMR is defined as the difference between the maximum and minimum values of the four SuperMAG ring current indices. See text for more details.

between 1000 local time (LT) and 1400 LT for each month during August 2001 to March 2016. The average data coverage is 31%. In order to overcome this shortage, we used the Huancayo magnetometer data, which provide a better coverage during the period of our investigation (see Figure 2b). It is known that the intensity of the equatorial electrojet, which can be estimated from the *H* component of the surface magnetic field, correlates well with V_Z (Anderson et al., 2002, 2004). Thus, once the relationship between V_Z and the equatorial electrojet intensity is determined, one can derive V_Z from *H*.

There are two ways to evaluate the equatorial electrojet intensity using ground-based magnetometer data. The first method involves two magnetometers: one magnetometer being right at the magnetic equator and the other magnetometer being in approximately the same longitude but several hundred kilometers away in the north or south from the magnetic equator (e.g., Manoj et al., 2006; Rastogi & Patil, 1986; Yizengaw et al., 2012, 2014). Since the equatorial electrojet is confined within $\pm 3^\circ$ from the magnetic equator, *H* at the magnetic equator is much more affected by the equatorial electrojet than *H* outside the equatorial electrojet belt. Meanwhile, magnetospheric currents affect *H* in the same way at the two locations because the spatial scale of magnetospheric currents is much greater than the distance between the two magnetometers. Therefore, the difference of *H* at the two locations is substantially free from the effect of magnetospheric currents but still contains the magnetic field produced by the equatorial electrojet. The deviation of this quantity from nighttime data, when the equatorial electrojet is vanishingly weak, gives a measure of the daytime equatorial electrojet intensity.

The other approach involves *H* from only one magnetometer close to the magnetic equator (Le Huy & Amory-Mazaudier, 2005; Siddiqui et al., 2015; Uozumi et al., 2008). The effect of large-scale magnetospheric currents is removed by subtracting a ring current index, such as *Dst*. After subtracting the nighttime baseline,

the residual in H represents the magnetic effect of the equatorial electrojet. The problem of this technique is that large-scale magnetospheric currents are not zonally symmetric when geomagnetic activity is very high (e.g., Love & Gannon, 2010), and thus, ring current indices fail to remove the effect of magnetospheric currents from H at individual stations (e.g., Olwendo et al., 2017).

We initially employed the two-station method using H from Huancayo and Piura, but the results were not satisfactory because of incompleteness and/or questionable quality of the Piura data in some months. Thus, the one-station method was preferred. Yamazaki and Maute (2017, pp. 324) presented a technique that simultaneously determines the effect of ring current and main field using a monthly record of H and the corresponding Dst index. For the present study, we have revised the technique and applied it to the H data from Huancayo. We used the SuperMAG ring current indices (Newell & Gjerloev, 2012) instead of the standard Dst index. The SuperMAG ring current indices consist of SMR-00, SMR-06, SMR-12, and SMR-18, which are computed in a similar way as the Dst index but separately derived for 0000, 0600, 1200, and 1800 magnetic local time sectors, based on 1-min magnetometer data collected from nearly 100 middle- and low-latitude SuperMAG stations (Gjerloev, 2012). We used the average of the four indices (denoted here as SMR) and the difference between the maximum and minimum values of the four indices (denoted here as ξSMR). As mentioned earlier, the one-station method tends to fail when the zonal asymmetry of magnetospheric currents is not negligible. Thus, the H data were discarded when ξSMR is larger than 20 nT. As in Yamazaki and Maute (2017), the data analysis was separately performed for each month of each year. After removing the data with $\xi\mathrm{SMR} > 20$ nT, we fitted SMR to the nighttime data ($\pm$2.5 hr from the midnight) of the same month and subtracted the fit from all the H data. The residual, denoted here as ΔH, is a measure of the equatorial electrojet intensity at Huancayo.

Figure 3 illustrates how our technique works using an example of December 2002. In Figure 3a, the black line shows 1-min H data from Huancayo. The green line indicates the periods when magnetospheric currents are highly asymmetric ($\xi\mathrm{SMR} > 20$ nT). Such periods are generally coincident with the times of relatively high geomagnetic activity, as shown in Figure 3c. The data with $\xi\mathrm{SMR} > 20$ nT are not used in the calculation of ΔH nor in the evaluation of the midday V_Z based on ΔH, which will be explained later. The red line in Figure 3a is the fit in the form $\alpha + \beta T + \gamma\mathrm{SMR}$ to the nighttime H data that are indicated by the blue "x" symbols. Here T is time in Julian days. The fitting coefficients α, β, and γ can be determined by the least squares method. There was a weak storm during this month, starting from 19 December 2002, and moderate-to-high geomagnetic activity lasted for many days (see Figure 3c). The minimum value of SMR was −74 nT, recorded on 21 December 2002. Figure 3b shows ΔH (i.e., H minus the SMR fit). ΔH tends to be positive during daytime, corresponding to the eastward flow of the equatorial electrojet, and around 0 during nighttime when the equatorial electrojet is essentially nonexistent. The large day-to-day variability in the daytime ΔH data is partly due to the response of the equatorial electrojet to variable magnetospheric forcing (e.g., Huang, 2012; Kikuchi et al., 2008; Yamazaki & Kosch, 2015) and also partly due to the effect of tides and planetary waves from the lower atmosphere (Kawano-Sasaki & Miyahara, 2008; Yamazaki, Richmond, Maute, Liu, et al., 2014).

The next step is to determine the quantitative relationship between ΔH and the equatorial vertical plasma drift velocity V_Z. For each month of each year, the JULIA V_Z measurements made between 1000 LT and 1400 LT were plotted against the corresponding values of ΔH. Figure 4a gives an example of such a plot for January 2013. It is evident that ΔH tends to increase with increasing V_Z. The coefficient of determination R^2, which is calculated as the square of the correlation coefficient, is 0.94. The average R^2 value derived from all the months during August 2001 to March 2016 is 0.84, including the best case R^2=0.97 and the worst case $R^2 = 0.62$. The green curve in Figure 4a shows the fit of ΔH to V_Z, which in this case is given as $V_Z = 1.55 \times 10^{-4}(\Delta H)^2 + 1.33 \times 10^{-1}(\Delta H) - 4.26$. The second-order term, that is, $(\Delta H)^2$, was necessary because of the apparent saturation of ΔH at high V_Z values. Alken and Maus (2010) discussed in detail how plasma instabilities in the equatorial ionosphere could occur under the presence of a large electric field, which leads to a saturation of the equatorial electrojet flow. It is also noted in Figure 4a that ΔH is not 0 but ~30 nT when V_Z is 0. A similar positive offset was also found for other months. The offset in ΔH at $V_Z = 0$ could arise from various reasons. For example, even if the zonal electric field is zero at heights of JULIA measurements (i.e., 150 km), the electric field could be nonzero at 100–110 km, where the equatorial electrojet flows. Also, the wind-driven current could exist even if the zonal electric field is zero.

Once the relationship between ΔH and V_Z was determined, the monthly mean value of ΔH was calculated at 1200 LT. The results were converted to the equivalent values in V_Z. In the case of January 2013, the monthly

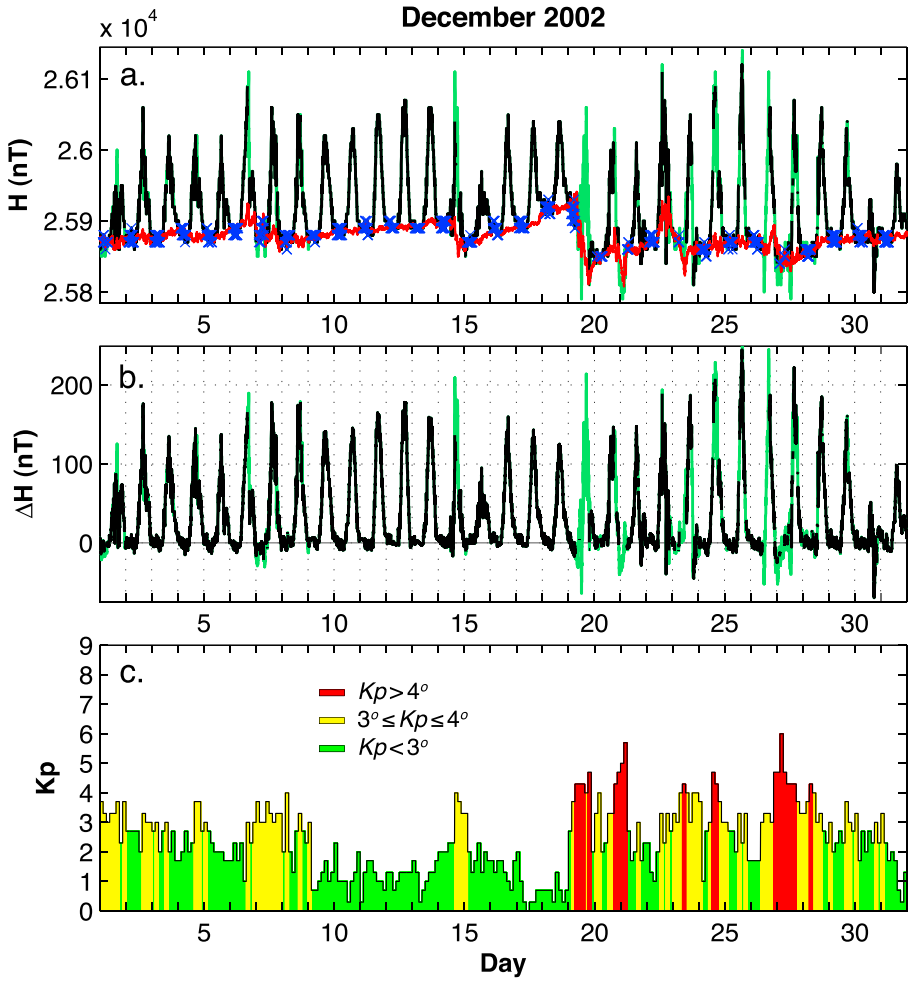

Figure 3. (a) *H* component magnetic field at Huancayo during December 2002. The black and green lines show 1-min data, corresponding the periods when large-scale magnetospheric currents are symmetric (ξSMR $\leq$ 20 nT) and asymmetric (ξSMR > 20 nT), respectively. The red line shows the fit of SMR to the nighttime data that are indicated by the blue "x" symbols (ξSMR $\leq$ 20 nT). (b) ΔH during the corresponding period, which is calculated as the difference between the *H* data and SMR fit. (c) Geomagnetic activity index *Kp*.

mean value of the noontime V_Z is 10.39 $\pm$ 1.14 m/s, as indicated in Figure 4a. Here the 1σ fitting error was estimated by the bootstrap method (Efron, 1981). In order to demonstrate the consistency between the results from the single-station method and those from the two-station method, we plot in Figures 4b–4d the relationship between V_Z and ΔH derived using the two station method. For the two-station method, the zero level of ΔH was set to be the monthly mean of the nighttime data ($\pm$2.5 hr from the midnight). Figures 4b–4d show the results derived with the Huancayo-Piura pair, Huancayo-Villa Remedios pair, and Huancayo-San Juan pair, respectively. The Quasi-Dipole latitude (e.g., Laundal & Richmond, 2017) is 0.18°N at Huancayo, 6.69°N at Piura, 5.20°S at Villa Remedios, and 26.58°N at San Juan, for January 2013. ΔH is different for different pairs of the stations, as the pattern of the daily variation in *H* is different at different stations. For instance, the range of daily variation in *H* is small at San Juan due to the proximity of the station to the S_q current focus (e.g., Campbell, 1982); thus, ΔH from the Huancayo-San Juan pair is similar to ΔH from the one-station method. ΔH from the Huancayo-Piura pair and the Huancayo-Villa Remedios pair are smaller. Nonetheless, there is a good correlation between V_Z and ΔH in all cases. The relatively large scatter in the results for the Huancayo-San Juan pair (Figure 4d) may be due to the large distance between Huancayo and San Juan (see Figure 1). The monthly mean of the noontime V_Z is 10.27 $\pm$ 1.54 m/s for the Huancayo-Piura pair, 11.73 $\pm$ 1.63 m/s for the Huancayo-Villa Remedios pair, and 9.45 $\pm$ 1.30 for the Huancayo-San Juan pair, which are all consistent with 10.39 $\pm$ 1.14 m/s derived from the one-station method.

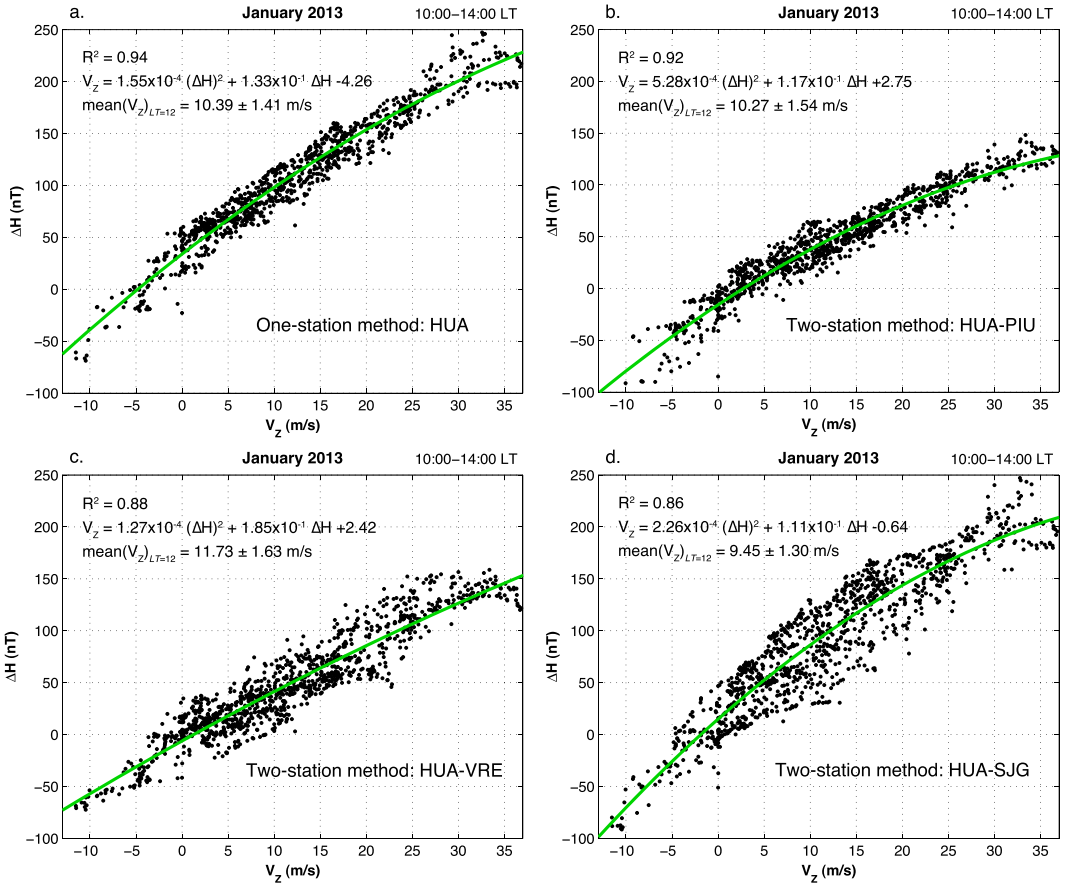

Figure 4. (a) Relationship between the daytime V_Z (1000–1400 local time, LT) from the Jicamarca Unattended Long-term Investigations of the Ionosphere and Atmosphere (JULIA) radar and the corresponding ΔH values from the Hucancayo magnetometer for January 2013. (b–d) The same as (a) except that ΔH values are derived by the two-station method. The pairs of stations used are as follows: (b) Huancayo (HUA) and Piura (PIU); (c) Huancayo and Villa Remedios (VRE); and (d) Huancayo and San Juan (SJG).

As a brief summary, both one-station and two-station methods are useful for evaluating V_Z from ΔH on a monthly basis. The advantage of the one-station method is the better long-term data coverage. The disadvantage is that the technique needs to be restricted to the periods when the large-scale magnetospheric currents are zonally symmetric, which is often not the case during storm events. Thus, the two-station method is preferable when studying the disturbed ionosphere in storm conditions, while the one-station method is more suitable for studying the long-term (>1 month) behavior of the average (or quiet) ionosphere. In the rest of the paper, we use V_Z derived from the one-station method, as it gives better data coverage than the two-station method.

4. Results

We plot in Figure 5a monthly mean values of the midday V_Z (black circles and line) during August 2001 to March 2016. Figure 5b shows the corresponding monthly values of the solar activity index P, which is defined as $P = (F_{10.7} + \overline{F_{10.7}})/2$, where $\overline{F_{10.7}}$ is the 81-day-centered average of the daily values of $F_{10.7}$ in solar flux unit (sfu = 10^{-22} W·m^{-2}·Hz^{-1}). The investigated period covers a solar cycle, including the maximum phase of solar cycle 23 (November 2001) and solar cycle 24 (April 2014).

The green dashed line in Figure 5a depicts the seasonal solar cycle climatology derived from the JULIA data. We constructed an empirical model of the midday V_Z using the JULIA measurements between 1130 LT and 1230 LT. Following the work of Alken (2009), the functional form of the model is given as follows:

$$V_Z(P, \mathrm{DoY}) = \sum_{i=1}^{2} \sum_{j=1}^{11} a_{ij} F_i(P) G_j(\mathrm{DoY}), \quad (1)$$

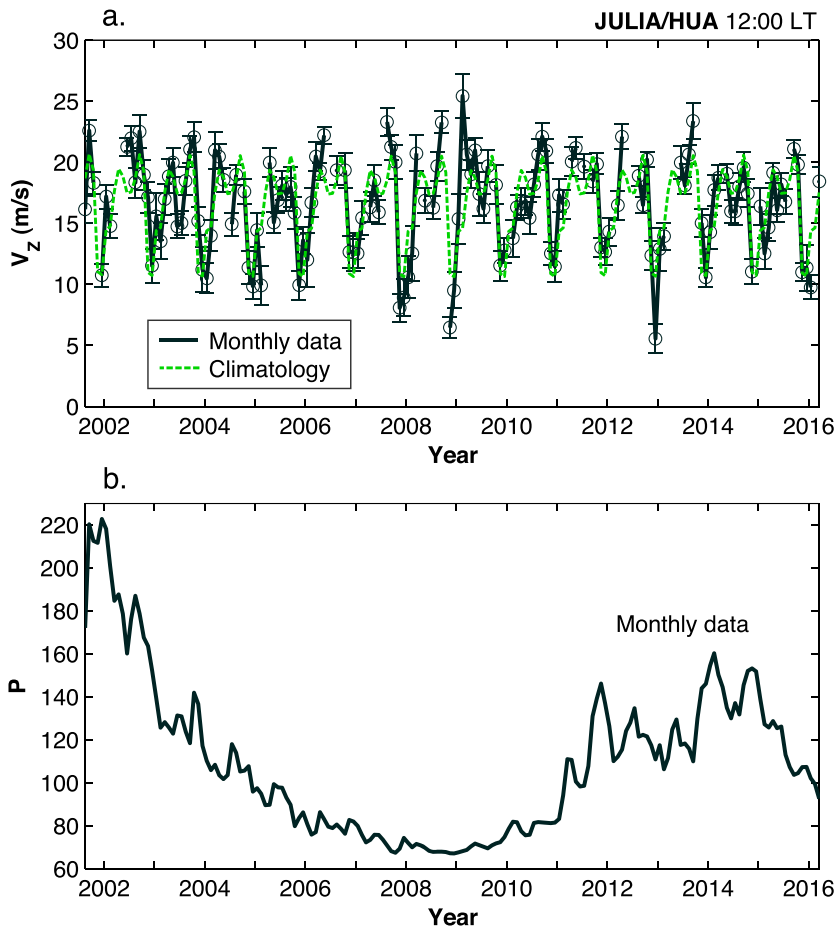

Figure 5. (a) Monthly mean values of the midday V_Z during 2001–2016. The seasonal solar cycle climatology derived from the Jicamarca Unattended Long-term Investigations of the Ionosphere and Atmosphere (JULIA) V_Z data based on equations (1)–(3) is also indicated by the green dashed line. (b) Monthly mean values of the solar activity index P. HUA = Huancayo; LT = local time.

where DoY is the day of year. The functions F_i and G_j are in the following form:

$$F_i(P) = P^{i-1} \tag{2}$$

$$\begin{aligned} G_j(\mathrm{DoY}) &= \cos\left(\frac{(j-1)\pi \mathrm{DoY}}{365.25}\right) \quad j \text{ odd} \\ &= \sin\left(\frac{(j-1)\pi \mathrm{DoY}}{365.25}\right) \quad j \text{ even} \end{aligned} \tag{3}$$

The model assumes a linear dependence of V_Z on P as well as the seasonal variation represented by Fourier functions up to degree 5. Unlike the model of Alken (2009), our model does not include the dependence on local time. This is because our data analysis is limited to a fixed local time range of 1130–1230 LT. The model coefficients a_{ij} were determined based on a least squares technique, using the measurements during geomagnetically quiet periods ($Kp < 3^{\circ}$).

Figure 6 presents the seasonal and solar activity dependence of V_Z derived from the JULIA observations (green dots) and model (red dashed line). In Figure 6a, the black line shows the 30-day running mean of the data, which is well reproduced by the model with $P = 110$ sfu, corresponding to the average value of P during the period of our investigation. In Figure 6b, the black circles are the average of the data for P <80, $80 \le P < 120$, $120 \le P < 160$, $160 \le P < 200$, and $200 \le P$ (in sfu). The red line shows the model prediction with DoY = 300, which happens to give a value close to the annal mean of V_Z. Neither model nor data reveals evidence for the solar activity effect on V_Z during 1130–1230 LT. The model results for different seasons similarly showed little

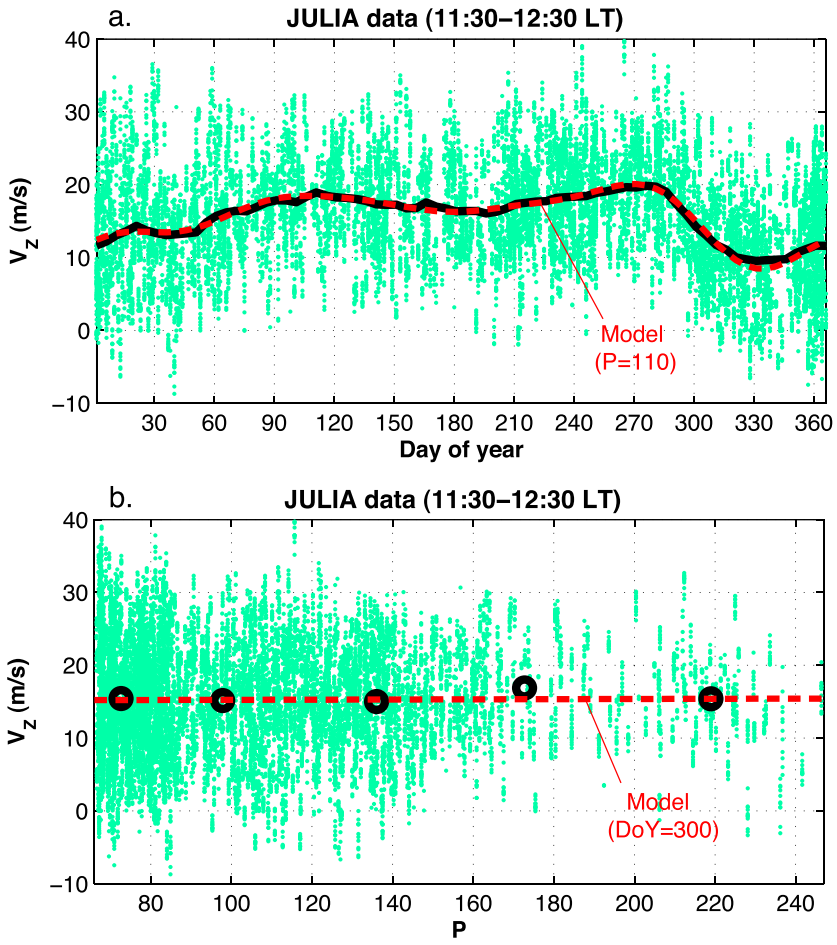

Figure 6. Dependence of V_Z on (a) season and (b) solar activity. In each panel, the green dots indicate the V_Z data from the Jicamarca Unattended Long-term Investigations of the Ionosphere and Atmosphere (JULIA) radar observed between 1130 local time (LT) and 1230 LT. In panel (a), the black line shows the 30-day running mean of the data, while the red dashed line shows the seasonal variation of V_Z obtained from our empirical model based on equations (1)–(3). In panel (b), the black circles are the average of the data for $P < 80$, $80 \le P < 120$, $120 \le P < 160$, $160 \le P < 200$, and $200 \le P$ (in sfu), while the red dashed line shows the solar activity dependence of V_Z obtained from the empirical model.

dependence on P. A similar analysis was also performed using daily values of $F_{10.7}$ instead of P. The results were very similar, showing no evidence for the solar activity dependence of V_Z.

Going back to Figure 5a, the month-to-month variability of the midday V_Z is dominated by the seasonal variation (~10 m/s), which is well reproduced by the model as indicated by the green dashed line. The seasonal pattern, characterized by two equinoctial maxima, is consistent with earlier results in the literature (Alken, 2009; Alken et al., 2013). Yamazaki, Richmond, Maute, Wu, et al. (2014) numerically showed that upward propagating tides from the lower atmosphere play an important role for the equinoctial maxima in the equatorial electrojet intensity.

The anomaly ΔV_Z, shown in Figure 7a, was calculated as the deviation of V_Z (black line in Figure 5a) from the seasonal solar cycle climatology (green dashed line in Figure 5a). Following Yamazaki et al. (2017), a moving average with a 13-month window was applied to ΔV_Z in order to extract the variation on time scales longer than a year. The results, shown in Figure 7a (red line), reveal an interannual variation of ~2 m/s. The variation pattern is very similar when a moving average with a 7-month window is used (Figure 7a, blue dashed line). Thus, the obtained results are not particularly sensitive to our choice of the window width for averaging.

Midday values of V_Z derived from GAIA were analyzed in the same way as the data. That is, the seasonal solar cycle dependence was first evaluated based on equations (1)–(3), and the residual from the climatology was calculated. ΔV_Z from GAIA, presented in Figure 7b, reproduces the observed pattern of the interannual

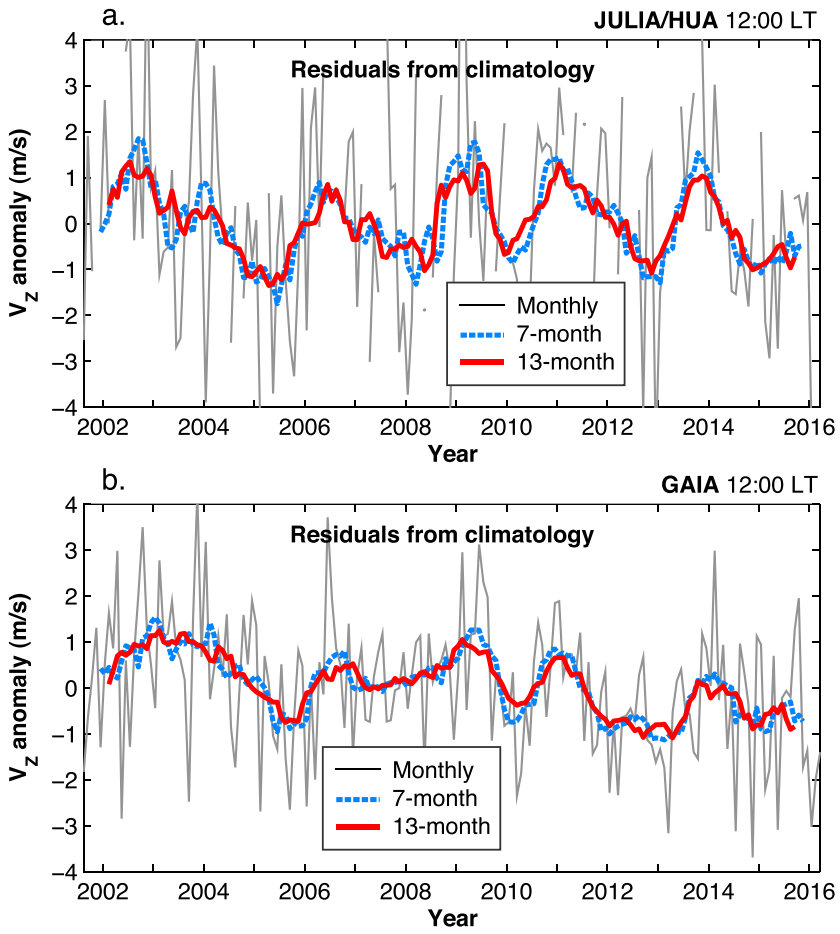

Figure 7. Anomaly ΔV_Z calculated as the deviation of V_Z from the seasonal solar cycle climatology derived from equations (1)–(3). The results are shown for (a) the observations and (b) GAIA model. The gray thin lines show monthly mean values, while the red and blue dashed lines show 13-month and 7-month smoothed values, respectively. JULIA = Jicamarca Unattended Long-term Investigations of the Ionosphere and Atmosphere; GAIA = Ground-to-topside Atmosphere-Ionosphere model for Aeronomy; HUA = Huancayo; LT = local time.

variation. Local maxima in 2006, 2009, 2011, and 2013 can be found in both observations (Figure 7a) and simulation results (Figure 7b). Although the pattern of the interannual variation is similar, the variability is larger in the observations compared to the GAIA results. It should also be noted that the GAIA model predicted an unrealistically large solar cycle variation in the midday values of V_Z (~4 m/s after the 13-month smoothing during August 2001 to March 2016). The reason for this is unclear. Since the solar activity influence is taken into account in equations (1)–(3), the anomaly ΔV_Z, shown in Figure 7b, is not affected by the overestimation of the solar activity dependence of V_Z in GAIA.

5. Discussion

We have shown that there is an interannual variation of ~2 m/s in the midday values of V_Z. In this section, we discuss potential sources of the variability. As we stated earlier, the ionosphere is subject to external forcing by energetic solar radiation, magnetospheric forcing, and wave forcing from the lower layers of the atmosphere. Although the 11-year variation of energetic solar radiation is an important driver of year-to-year variations for many ionospheric parameters, we did not observe any obvious solar cycle influence on V_Z at 1200 LT (Figure 6b). During August 2001 to March 2016, monthly values of the P index varied in the range of 67–223 sfu (see Figure 5b). The difference of the midday V_Z at $P = 67$ sfu and $P = 223$ sfu estimated from our model based on equations (1)–(3) is 0.19 m/s, which is smaller than the 1σ error (= 0.22 m/s) estimated using the bootstrap technique. The results suggest that the solar cycle contribution to the interannual variability of V_Z is negligible at 1200 LT. The absence of, or very small, solar cycle influence on the daytime V_Z is

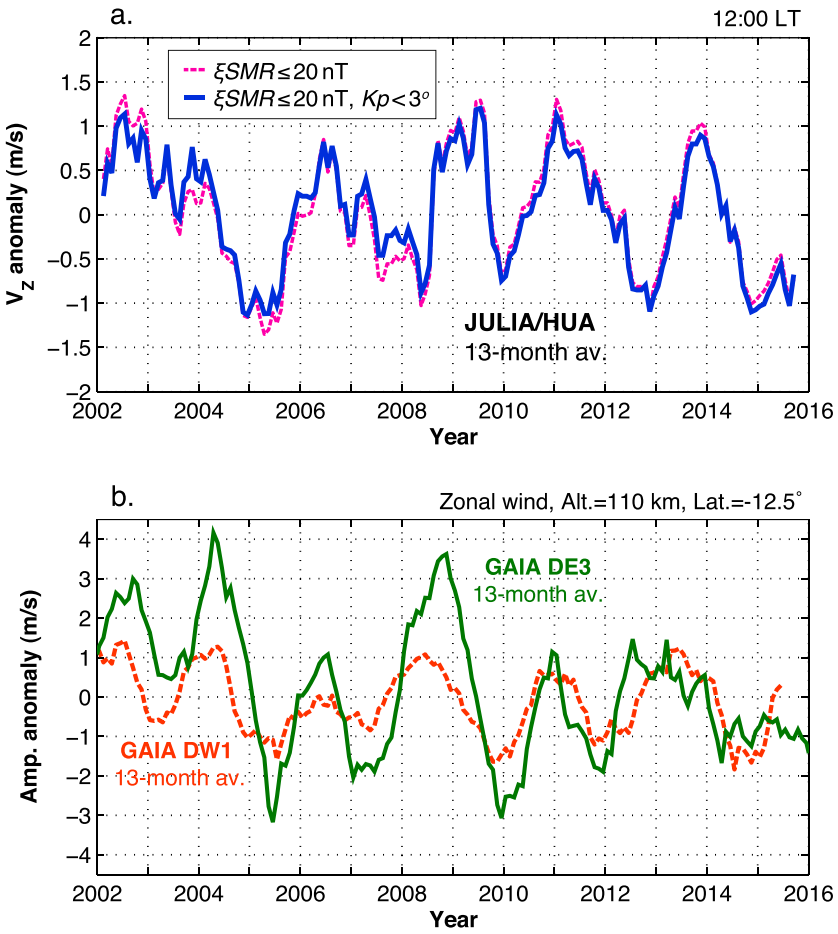

Figure 8. (a) Interannual variations of V_Z. The blue line shows the result derived using only quiet time ($Kp < 3°$) data. The magenta dashed line is the same as the red line in Figure 7a. (b) Interannual variations in the amplitude of the migrating diurnal tide (DW1) and eastward propagating nonmigrating tide with zonal wave number 3 (DE3) from GAIA. JULIA = Jicamarca Unattended Long-term Investigations of the Ionosphere and Atmosphere; GAIA = Ground-to-topside Atmosphere-Ionosphere model for Aeronomy; HUA = Huancayo; LT = local time.

consistent with earlier studies (e.g., Fejer et al., 2008; Richmond et al., 2015; Scherliess & Fejer, 1999). These studies also showed that the effect of solar activity on V_Z depends largely on local time. It is well known that the solar activity dependence of V_Z is particularly strong around the time of prereversal enhancement (1800–1900 LT).

The magnetospheric influence is also considered to be small, given that the GAIA model was able to reproduce the pattern of the interannual variation without variable magnetospheric forcing. As shown in Figure 8a, the pattern of the interannual variation is largely the same when the investigation is strictly limited to geomagnetically quiet periods ($Kp < 3°$ as well as ξSMR $\leq$ 20 nT). This further supports that magnetospheric forcing does not make a significant contribution to the observed interannual variation of V_Z at 1200 LT.

There is a possible contribution from the change in the Earth's main magnetic field **B**. At the JULIA location, the strength of the geomagnetic field decreased by approximately 4% during 2001–2016. Changes in the strength of the geomagnetic field can affect the ionospheric electrodynamics (Cnossen & Richmond, 2013; Takeda, 1996). Recently, Tao et al. (2017), using the GAIA model, examined the response of various ionospheric parameters to the reduction of the dipole magnetic moment. They performed a simulation with the magnetic dipole moment of 7.8×10^{22} Am^2 as the base case and compared the results with other simulations in which the magnetic dipole moment was reduced to 75%, 50%, and 10% of the base case. We also evaluated the change in V_Z due to the 4% reduction of the magnetic field strength during 2001–2016 using GAIA. The change in V_Z was found to be very small (<0.1 m/s).

Acknowledgments
We would like to thank Yang-Yi Sun for his support in retrieving the GAIA V_Z data. The GAIA data used in this paper will be made available upon request to Y. Y. We would also like thank Gabriel Brando Soares for his help in plotting the map of stations. The results presented in this paper partly rely on the data from the Jicamarca Observatory. The Jicamarca Observatory is a facility of the Instituto Geofisico del Peru (IGP) operated with support from the NSF AGS-905448 through the Cornell University. The radar data used are available at jro.igp.gob.pe/madrigal. Our results also partly rely on the magnetic data collected at Huancayo and San Juan. We thank IGP and United States Geophysical Survey (USGS) for supporting the operation. We acknowledge the INTERMAGNET (www.intermagnet.org/) and WDC for Geomagnetism, Edinburgh (www.wdc.bgs.ac.uk/) for distributing the data. We also thank the German Research Centre for Geosciences (GFZ) and Universidad Mayor de San Andres (UMSA) for the operation of the magnetometer at Villa Remedios. The Piura data were made available by the LISN project (lisn.igp.gob.pe/), which is led by the University of Texas at Dallas in collaboration with the Geophysical Institute of Peru, and other institutions that provide information in benefit of the scientific community. For the SuperMAG data, we gratefully acknowledge: INTERMAGNET; USGS, Jeffrey J. Love; CARISMA, PI Ian Mann; CANMOS; The S-RAMP Database, PI K. Yumoto, and K. Shiokawa; The SPIDR database; AARI, PI Oleg Troshichev; The MACCS program, PI M. Engebretson, Geomagnetism Unit of the Geological Survey of Canada; GIMA; MEASURE, UCLA IGPP and Florida Institute of Technology; SAMBA, PI Eftyhia Zesta; 210 Chain, PI K. Yumoto; SAMNET, PI Farideh Honary; The institutes who maintain the IMAGE magnetometer array, PI Eija Tanskanen; PENGUIN; AUTUMN, PI Martin Connors; DTU Space, PI Rico Behlke; South Pole and McMurdo Magnetometer, PI's Louis J. Lanzarotti and Alan T. Weatherwax; ICESTAR; RAPIDMAG; PENGUIn; British Artarctic Survey; McMac, PI Peter Chi; BGS, PI Susan Macmillan; Pushkov Institute of Terrestrial Magnetism, Ionosphere and Radio Wave Propagation (IZMIRAN); GFZ, PI Juergen Matzka; MFGI, PI B. Heilig; IGFPAS, PI J. Reda; University of L'Aquila, PI M. Vellante; BCMT, V. Lesur and A. Chambodut; Data obtained in cooperation with Geoscience Australia, PI Marina Costelloe; SuperMAG, PI Jesper W. Gjerloev. The *Kp* index was provided by GFZ Potsdam, available at www.gfz-potsdam.de/en/kp-index/. The $F_{10.7}$ index was provided by the

Our results rule out the dominant contribution from solar and magnetospheric forcing, as well as from the Earth's main magnetic field, to the observed interannual variation of V_Z. It is, therefore, likely that the interannual variation of V_Z at 1200 LT is mainly driven by lower atmospheric forcing. One possible mechanism that enables lower atmospheric effects on the ionosphere is the modulation of the daytime equatorial electric field by atmospheric tides (e.g., Millward et al., 2001; Yamazaki & Richmond, 2013). The tidal waves that propagate to the ionosphere from below have been observed to vary from year to year (e.g., Forbes et al., 2008; Oberheide et al., 2009; Vincent et al., 1998; Wu et al., 2008). The interannual variability of upward propagating tides is due in part to the interannual variability of the background atmosphere, through which the tidal waves propagate (Mayr & Mengel, 2005; McLandress, 2002). Some identified sources of the interannual variability of tides include the QBO in the stratosphere (Liu, 2014; Yamazaki et al., 2017) and the El Niño–Southern Oscillation (ENSO) in the troposphere (Liu et al., 2017; Pedatella & Liu, 2012; 2013). The QBO has a regular oscillation cycle of ~28 months, while ENSO consists of longer-period oscillations (~43 and ~62 months) (Liu, 2016b). Yamazaki et al. (2017) examined the interannual variability of tides at dynamo region altitudes during 1997–2016 using GAIA. We show in Figure 8b the interannual variation in the amplitude of the migrating diurnal tide "DW1" (orange dashed line) and the eastward propagating nonmigrating diurnal tide with zonal wave number 3 "DE3" (green line) in the zonal wind at 12.5°S latitude at 110 km height derived from GAIA. As discussed in Yamazaki et al. (2017), the interannual variations of these tidal modes are under a significant influence of the stratospheric QBO. Yamazaki et al. (2017) pointed out that the interannual variability of tides in GAIA was somewhat smaller compared to observations, which may explain the smaller interannual variability of V_Z in GAIA than in data (Figure 7). Although the comparison of Figures 8a and 8b reveals some resemblance between the interannual variations of V_Z and tidal amplitudes, there is no one-to-once correspondence. Further studies are required to clarify the effect of tides and other atmospheric waves on the interannual variability of the equatorial ionospheric electric field. Similar observations from other longitudinal sectors (e.g., Patra et al., 2014) would be useful for the identification of the waves involved. Also, it needs to be investigated how the plasma density in the low-latitude ionosphere responds to the interannual variation of the equatorial electric field. According to the empirical formula presented by Stolle et al. (2008), an increase of V_Z by 2 m/s can cause an increase in the crest-to-trough ratio of the EIA by approximately 5%, which might be detectable. Previous studies found a quasi 2-year variation in the ionospheric plasma density (e.g., Chang et al., 2016; Chen, 1992; Echer, 2007; Kane, 1995; Tang et al., 2014; Zhou et al., 2016). The role of the equatorial electric field is yet to be examined.

6. Conclusions

The main results of the present study may be summarized as follows:

1. Monthly mean values of the equatorial vertical plasma drift velocity V_Z at 1200 LT during 2001–2016 are dominated by a seasonal variation of ~10 m/s and show no significant dependence on solar activity as represented by the *P* index. After the removal of the seasonal variation, the V_Z data reveal an interannual variation of ~2 m/s, which has an oscillation period of 2–3 years.
2. The pattern of the interannual variation is reproduced by the GAIA model that takes into account realistic interannual variability of the atmosphere below 30 km but ignores interannual variability of the magnetosphere. Thus, it is likely that the observed interannual variation of V_Z at 1200 LT is mainly driven by atmospheric forcing from below. The atmospheric process that is responsible for the interannual variability of V_Z remains to be identified. It is noticed that the interannual variation of V_Z shows some resemblance with those in atmospheric tides.

References

Alken, P. (2009). A quiet time empirical model of equatorial vertical plasma drift in the Peruvian sector based on 150 km echoes. *Journal of Geophysical Research*, *114*, A02308. https://doi.org/10.1029/2008JA013751

Alken, P., Chulliat, A., & Maus, S. (2013). Longitudinal and seasonal structure of the ionospheric equatorial electric field. *Journal of Geophysical Research: Space Physics*, *118*, 1298–1305. https://doi.org/10.1029/2012JA018314

Alken, P., & Maus, S. (2007). Spatio-temporal characterization of the equatorial electrojet from CHAMP, Ørsted, and SAC-C satellite magnetic measurements. *Journal of Geophysical Research*, *112*, A09305. https://doi.org/10.1029/2007JA012524

Alken, P., & Maus, S. (2010). Relationship between the ionospheric eastward electric field and the equatorial electrojet. *Geophysical Research Letters*, *37*, L04104. https://doi.org/10.1029/2009GL041989

Anderson, D., Anghel, A., Chau, J., & Veliz, O. (2004). Daytime vertical E×B drift velocities inferred from ground- based magnetometer observations at low latitudes. *Space Weather*, *2*, S11001. https://doi.org/10.1029/2004SW000095

Natural Resources Canada, available at www.spaceweather.ca/solarflux/sx-en.php. JVDM can be downloaded from the CIRES website at geomag.org/models/JVDM.html. C. S. and J. M. were partly supported by the Priority Program 1788 "Dynamic Earth" of Deutsche Forschungsgemeinschaft (DFG). H. L. acknowledges support from JSPS KAKENHI grants 15K05301, 15H02135, and 15H03733. C. T. was partly supported by MEXT/JSPS KAKENHI grants 15H05813, 15H05815, and 15H05816. Y. Y. was supported by the Humboldt Research Fellowship for Experienced Researchers from the Alexander von Humboldt Foundation.

Anderson, D., Anghel, A., Yumoto, K., Ishitsuka, M., & Kudeki, E. (2002). Estimating daytime vertical E×B drift velocities in the equatorial *F*-region using ground-based magnetometer observations. *Geophysical Research Letters*, *29*(12), 1596. https://doi.org/10.1029/2001GL014562

Baldwin, M. P., Gray, L. J., Dunkerton, T. J., Hamilton, K., Haynes, P. H., Randel, W. J., et al. (2001). The quasi-biennial oscillation. *Reviews of Geophysics*, *39*, 179–229.

Balsley, B. B. (1973). Electric fields in the equatorial ionosphere: A review of techniques and measurements. *Journal of Atmospheric and Terrestrial Physics*, *35*, 1035–1044. https://doi.org/10.1016/0021-9169(73) 90003-2

Bilitza, D., Altadill, D., Zhang, Y., Mertens, C., Truhlik, V., Richards, P., et al. (2014). The International Reference Ionosphere 2012: A model of international collaboration. *Journal of Space Weather and Space Climate*, *4*, A07. https://doi.org/10.1051/swsc/2014004

Campbell, W. H. (1982). Annual and semiannual changes of the quiet daily variations (Sq) in the geomagnetic field at North American locations. *Journal of Geophysical Research*, *87*(A2), 785–796. https://doi.org/10.1029/JA087iA02p00785

Chang, L. C., Sun, Y.-Y., Yue, J., Wang, J. C., & Chien, S.-H. (2016). Coherent seasonal, annual, and quasi-biennial variations in ionospheric tidal/SPW amplitudes. *Journal of Geophysical Research: Space Physics*, *121*, 6970–6985. https://doi.org/10.1002/2015JA022249

Chau, J. L., Aponte, N. A., Cabassa, E., Sulzer, M. P., Goncharenko, L. P., & González, S. A. (2010). Quiet time ionospheric variability over Arecibo during sudden stratospheric warming events. *Journal of Geophysical Research*, *115*, A00G06. https://doi.org/10.1029/2010JA015378

Chau, J. L., & Kudeki, E. (2006). Statistics of 150-km echoes over Jicamarca based on low-power VHF observations. *Annales de Geophysique*, *24*, 1305–1310.

Chau, J. L., & Woodman, R. F. (2004). Daytime vertical and zonal velocities from 150-km echos: Their relevance to *F*-region dynamics. *Geophysical Research Letters*, *31*, L17801. https://doi.org/10.1029/2004GL020800

Chen, P.-R. (1992). Evidence of the ionospheric response to the QBO. *Geophysical Research Letters*, *19*, 1089–1092.

Cnossen, I., & Richmond, A. D. (2013). Changes in the Earth's magnetic field over the past century: Effects on the ionosphere-thermosphere system and solar quiet (Sq) magnetic variation. *Journal of Geophysical Research: Space Physics*, *118*, 849–858. https://doi.org/10.1029/2012JA018447

Du, J., & Stening, R. J. (1999). Simulating the ionospheric dynamo, II, Equatorial electric fields. *Journal of Atmospheric and Solar-Terrestrial Physics*, *61*, 925–940.

Echer, E. (2007). On the quasi-biennial oscillation (QBO) signal in the foF2 ionospheric parameter. *Journal of Atmospheric and Solar-Terrestrial Physics*, *69*, 621–627.

Efron, B. (1981). Nonparametric estimates of standard error: The jackknife, the bootstrap, and other methods. *Biometrika*, *68*(3), 589–59.

Fang, T.-W., Akmaev, R., Fuller-Rowell, T., Wu, F., Maruyama, N., & Millward, G. (2013). Longitudinal and day-to-day variability in the ionosphere from lower atmosphere tidal forcing. *Geophysical Research Letters*, *40*, 2523–2528. https://doi.org/10.1002/grl.50550

Fejer, B. G. (1981). The equatorial ionospheric electric fields: A review. *Journal of Atmospheric and Terrestrial Physics*, *53*, 377–383.

Fejer, B. G., Farley, D. T., Woodman, R. F., & Calderon, C. (1979). Dependence of equatorial F region vertical drifts on season and solar cycle. *Journal of Geophysical Research*, *84*, 5792–5796.

Fejer, B. G., Jensen, J. W., & Su, S.-Y. (2008). Quiet time equatorial *F* region vertical plasma drift model derived from ROCSAT-1 observations. *Journal of Geophysical Research*, *113*, A05304. https://doi.org/10.1029/2007JA012801

Forbes, J. M., Zhang, X., Palo, S., Russell, J., Mertens, C. J., & Mlynczak, M. (2008). Tidal variability in the ionospheric dynamo region. *Journal of Geophysical Research*, *113*, A02310. https://doi.org/10.1029/2007JA012737

Fuller-Rowell, T. J., Codrescu, M. V., Moffett, R. J., & Quegan, S. (1994). Response of the thermosphere and ionosphere to geomagnetic storms. *Journal of Geophysical Research*, *99*, 3893–3914. https://doi.org/10.1029/93JA02015

Gjerloev, J. W. (2012). The SuperMAG data processing technique. *Journal of Geophysical Research*, *117*, A09213. https://doi.org/10.1029/2012JA017683

Goncharenko, L. P., Chau, J. L., Liu, H.-L., & Coster, A. J. (2010). Unexpected connections between the stratosphere and ionosphere. *Geophysical Research Letters*, *37*, L10101. https://doi.org/10.1029/2010GL043125

Goncharenko, L. P., Coster, A. J., Chau, J. L., & Valladares, C. E. (2010). Impact of sudden stratospheric warmings on equatorial ionization anomaly. *Journal of Geophysical Research*, *115*, A00G07. https://doi.org/10.1029/2010JA015400

Hanson, W. B., & Moffett, R. J. (1966). Ionization transport effects in the equatorial *F* region. *Journal of Geophysical Research*, *71*(23), 5559–5572. https://doi.org/10.1029/JZ071i023p05559

Huang, C.-S. (2012). Statistical analysis of dayside equatorial ionospheric electric fields and electrojet currents produced by magnetospheric substorms during sawtooth events. *Journal of Geophysical Research*, *117*, A02316. https://doi.org/10.1029/2011JA017398

Hysell, D. L., Larsen, M. F., & Woodman, R. F. (1997). JULIA radar studies of electric fields in the equatorial electrojet. *Geophysical Research Letters*, *24*, 1687–1690.

Jee, G., Schunk, R. W., & Scherliess, L. (2004). Analysis of TEC data from the TOPEX/Poseidon mission. *Journal of Geophysical Research*, *109*, A01301. https://doi.org/10.1029/2003JA010058

Jin, H., Miyoshi, Y., Fujiwara, H., & Shinagawa, H. (2008). Electrodynamics of the formation of ionospheric wave number 4 longitudinal structure. *Journal of Geophysical Research*, *113*, A09307. https://doi.org/10.1029/2008JA013301

Jin, H., Miyoshi, Y., Fujiwara, H., Shinagawa, H., Terada, K., Terada, N., et al. (2011). Vertical connection from the tropospheric activities to the ionospheric longitudinal structure simulated by a new Earth's whole atmosphere-ionosphere coupled model. *Journal of Geophysical Research*, *116*, A01316. https://doi.org/10.1029/2010JA015925

Jin, H., Miyoshi, Y., Pancheva, D., Mukhtarov, P., Fujiwara, H., & Shinagawa, H. (2012). Response of migrating tides to the stratospheric sudden warming in 2009 and their effects on the ionosphere studied by a whole atmosphere-ionosphere model GAIA with COSMIC and TIMED/SABER observations. *Journal of Geophysical Research*, *117*, A10323. https://doi.org/10.1029/2012JA017650

Kane, R. P. (1995). Quasi-biennial oscillation in ionospheric parameters measured at Juliusruh (55°N, 13°E). *Journal of Atmospheric and Terrestrial Physics*, *57*, 415–419.

Kawano-Sasaki, K., & Miyahara, S. (2008). A study on three-dimensional structures of the ionospheric dynamo currents induced by the neutral winds simulated by the Kyushu-GCM. *Journal of Atmospheric and Solar-Terrestrial Physics*, *70*, 1549–1562.

Kikuchi, T., Hashimoto, K. K., & Nozaki, K. (2008). Penetration of magnetospheric electric fields to the equator during a geomagnetic storm. *Journal of Geophysical Research*, *113*, A06214. https://doi.org/10.1029/2007JA012628

Kil, H., Oh, S.-J., Kelley, M. C., Paxton, L. J., England, S. L., Talaat, E., et al. (2007). Longitudinal structure of the vertical E×B drift and ion density seen from ROCSAT-1. *Geophysical Research Letters*, *34*, L14110. https://doi.org/10.1029/2007GL030018

Kobayashi, S., Ota, Y., Harada, Y., Ebita, A., Moriya, M., Onoda, H., et al. (2015). The JRA-55 reanalysis: General specifications and basic characteristics. *Journal of the Meteorological Society of Japan*, *93*, 5–48. https://doi.org/10.2151/jmsj.2015-001

Kudeki, E., & Fawcett, C. D. (1993). High resolution observations of 150 km echos at Jicamarca. *Geophysical Research Letters*, *20*, 1987–1990.

Laundal, K. M., & Richmond, A. D. (2017). Magnetic coordinate systems. *Space Science Reviews*, *206*, 27–59. https://doi.org/10.1007/s11214-016-0275-y

Le Huy, M., & Amory-Mazaudier, C. (2005). Magnetic signature of the ionospheric disturbance dynamo at equatorial latitudes: "D_{dyn}". *Journal of Geophysical Research*, *110*, A10301. https://doi.org/10.1029/2004JA010578

Lean, J. L., Emmert, J. T., Picone, J. M., & Meier, R. R. (2011). Global and regional trends in ionospheric total electron content. *Journal of Geophysical Research*, *116*, A00H04. https://doi.org/10.1029/2010JA016378

Li, K.-F., Lin, L.-C., Bui, X.-H., & Liang, M.-C. (2018). The 11 year solar cycle response of the equatorial ionization anomaly observed by GPS radio occultation. *Journal of Geophysical Research: Space Physics*, *123*, 848–861. https://doi.org/10.1002/2017JA024634

Lin, C. H., Liu, J. Y., Fang, T. W., Chang, P. Y., Tsai, H. F., Chen, C. H., & Hsiao, C. C. (2007). Motions of the equatorial ionization anomaly crests imaged by FORMOSAT-3/COSMIC. *Geophysical Research Letters*, *34*, L19101. https://doi.org/10.1029/2007GL030741

Lin, C. H., Richmond, A. D., Liu, J. Y., Yeh, H. C., Paxton, L. J., & Lu, G. (2005). Large-scale variations of the low-latitude ionosphere during the October–November 2003 superstorm: Observational results. *Journal of Geophysical Research*, *110*, A09S28. https://doi.org/10.1029/2004JA010900

Liu, H.-L. (2014). WACCM-X simulation of tidal and planetary wave variability in the upper atmosphere. In J. Huba, R. Schunk, & G. Khazanov (Eds.), *Modeling the ionosphere-thermosphere system*. Chichester, UK: John Wiley. https://doi.org/10.1002/9781118704417.ch16

Liu, H.-L. (2016a). Variability and predictability of the space environment as related to lower atmosphere forcing. *Space Weather*, *14*, 634–658. https://doi.org/10.1002/2016SW001450

Liu, H. (2016b). Thermospheric inter-annual variability and its potential connection to ENSO and stratospheric QBO. *Earth, Planets and Space*, *68*, 77. https://doi.org/10.1186/s40623-016-0455-8

Liu, H., Jin, H., Miyoshi, Y., Fujiwara, H., & Shinagawa, H. (2013). Upper atmosphere response to stratosphere sudden warming: Local time and height dependence simulated by GAIA model. *Geophysical Research Letters*, *40*, 635–640. https://doi.org/10.1002/grl.50146

Liu, H., Stolle, C., Förster, M., & Watanabe, S. (2007). Solar activity dependence of the electron density in the equatorial anomaly regions observed by CHAMP. *Journal of Geophysical Research*, *112*, A11311. https://doi.org/10.1029/2007JA012616

Liu, H., Sun, Y.-Y., Miyoshi, Y., & Jin, H. (2017). ENSO effects on MLT diurnal tides: A 21 year reanalysis data-driven GAIA model simulation. *Journal of Geophysical Research: Space Physics*, *122*, 5539–5549. https://doi.org/10.1002/2017JA024011

Liu, H., Yamamoto, M., Tulasi Ram, S., Tsugawa, T., Otsuka, Y., Stolle, C., et al. (2011). Equatorial electrodynamics and neutral background in the Asian sector during the 2009 stratospheric sudden warming. *Journal of Geophysical Research*, *116*, A08308. https://doi.org/10.1029/2011JA016607

Love, J. J., & Chulliat, A. (2013). An international network of magnetic observatories. *Eos Transactions American Geophysical Union*, *94*(42), 373–384. https://doi.org/10.1002/2013EO420001

Love, J. J., & Gannon, J. L. (2010). Movie-maps of low-latitude magnetic storm. *Space Weather*, *8*, S06001. https://doi.org/10.1029/2009SW000518

Lu, G., Hagan, M. E., Häusler, K., Doornbos, E., Bruinsma, S., Anderson, B. J., & Korth, H. (2014). Global ionospheric and thermospheric response to the 5 April 2010 geomagnetic storm: An integrated data-model investigation. *Journal of Geophysical Research: Space Physics*, *119*, 10,358–10,375. https://doi.org/10.1002/2014JA020555

Lühr, H., Maus, S., & Rother, M. (2004). Noon-time equatorial electrojet: Its spatial features as determined by the CHAMP satellite. *Journal of Geophysical Research*, *109*, A01306. https://doi.org/10.1029/2002JA009656

Manoj, C., Lühr, H., Maus, S., & Nagarajan, N. (2006). Evidence for short spatial correlation lengths of the noontime equatorial electrojet inferred from a comparison of satellite and ground magnetic data. *Journal of Geophysical Research*, *111*, A11312. https://doi.org/10.1029/2006JA011855

Matzka, J., Ricaldi, E., & Miranda, P. (2018). Preliminary minute mean values of geomagnetic observatory Ville Remedios, Bolivia, for January 2013. V. 1.0. http://doi.org/10.5880/GFZ.2.3.2018.001

Matzka, J., Siddiqui, T. A., Lilienkamp, H., Stolle, C., & Veliz, O. (2017). Quantifying solar flux and geomagnetic main field influence on the equatorial ionospheric current system at the geomagnetic observatory Huancayo. *Journal of Atmospheric and Solar-Terrestrial Physics*, *163*, 120–125. https://doi.org/10.1016/j.jastp.2017.04.014

Maute, A., Fejer, B. G., Forbes, J. M., Zhang, X., & Yudin, V. (2016). Equatorial vertical drift modulation by the lunar and solar semidiurnal tides during the 2013 sudden stratospheric warming. *Journal of Geophysical Research: Space Physics*, *121*, 1658–1668. https://doi.org/10.1002/2015JA022056

Maute, A., Richmond, A. D., & Roble, R. G. (2012). Sources of low-latitude ionospheric E×B drifts and their variability. *Journal of Geophysical Research*, *117*, A06312. https://doi.org/10.1029/2011JA017502

Mayr, H. G., & Mengel, J. G. (2005). Interannual variations of the diurnal tide in the mesosphere generated by the quasi-biennial oscillation. *Journal of Geophysical Research*, *110*, D10111. https://doi.org/10.1029/2004JD005055

McLandress, C. (2002). Interannual variations of the diurnal tide in the mesosphere induced by a zonal-mean wind oscillation in the tropics. *Geophysical Research Letters*, *29*(9), 1305. https://doi.org/10.1029/2001GL014551

Millward, G. H., Müller-Wodarg, I. C. F., Aylward, A. D., Fuller-Rowell, T. J., Richmond, A. D., & Moffett, R. J. (2001). An investigation into the influence of tidal forcing on *F* region equatorial vertical ion drift using a global ionosphere-thermosphere model with coupled electrodynamics. *Journal of Geophysical Research*, *106*(A11), 24,733–24,744. https://doi.org/10.1029/2000JA000342

Miyoshi, Y., Fujiwara, H., Jin, H., Shinagawa, H., & Liu, H. (2012). Numerical simulation of the equatorial wind jet in the thermosphere. *Journal of Geophysical Research*, *117*, A03309. https://doi.org/10.1029/2011JA017373

Miyoshi, Y., Pancheva, D., Mukhtarov, P., Jin, H., Fujiwara, H., & Shinagawa, H. (2017). Excitation mechanism of non-migrating tides. *Journal of Atmospheric and Solar-Terrestrial Physics*, *156*, 24–36. https://doi.org/10.1016/j.jastp.2017.02.012

Mukhtarov, P., Andonov, B., & Pancheva, D. (2013). Global empirical model of TEC response to geomagnetic activity. *Journal of Geophysical Research: Space Physics*, *118*, 6666–6685. https://doi.org/10.1002/jgra.50576

Mukhtarov, P., Pancheva, D., Andonov, B., & Pashova, L. (2013). Global TEC maps based on GNSS data: 1. Empirical background TEC model. *Journal of Geophysical Research: Space Physics*, *118*, 4594–4608. https://doi.org/10.1002/jgra.50413

Nava, B., Rodríguez-Zuluaga, J., Alazo- Cuartas, K., Kashcheyev, A., Migoya-Orué, Y., Radicella, S. M., et al. (2016). Middle- and low-latitude ionosphere response to 2015 St. Patrick's Day geomagnetic storm. *Journal of Geophysical Research: Space Physics*, *121*, 3421–3438. https://doi.org/10.1002/2015JA022299

Newell, P. T., & Gjerloev, J. W. (2012). SuperMAG-based partial ring current indices. *Journal of Geophysical Research*, *117*, A05215. https://doi.org/10.1029/2012JA017586

Oberheide, J., Forbes, J. M., Häusler, K., Wu, Q., & Bruinsma, S. L. (2009). Tropospheric tides from 80 to 400 km: Propagation, interannual variability, and solar cycle effects. *Journal of Geophysical Research*, *114*, D00I05. https://doi.org/10.1029/2009JD012388

Oberheide, J., Shiokawa, K., Gurubaran, S., Ward, W. E., Fujiwara, H., Kosch, M. J., et al. (2015). The geospace response to variable inputs from the lower atmosphere: A review of the progress made by Task Group 4 of CAWSES-II. *Progress in Earth and Planetary Science*, *2*, 2. https://doi.org/10.1186/s40645-014-0031-4

Olwendo, O. J., Cesaroni, C., Yamazaki, Y., & Cilliers, P. (2017). Equatorial ionospheric disturbances over the East African sector during the 2015 St. Patrick's day storm. *Advances in Space Research*, *60*, 1817–1826.

Onogi, K., Tsutsui, J., Koide, H., Sakamoto, M., Kobayashi, S., Hatsushika, H., et al. (2007). The JRA-25 reanalysis. *Journal of the Meteorological Society of Japan*, *85*, 369–432. https://doi.org/10.2151/jmsj.85.369

Patra, A. K., Chaitanya, P. P., Otsuka, Y., Yokoyama, T., Yamamoto, M., Stoneback, R. A., & Heelis, R. A. (2014). Vertical ExB drifts from radar and C/NOFS observations in the Indian and Indonesian sectors: Consistency of observations and model. *Journal of Geophysical Research: Space Physics*, *119*, 3777–3788. https://doi.org/10.1002/2013JA019732

Pedatella, N. M., & Liu, H.-L. (2012). Tidal variability in the mesosphere and lower thermosphere due to the El Niño–Southern Oscillation. *Geophysical Research Letters*, *39*, L19802. https://doi.org/10.1029/2012GL053383

Pedatella, N. M., & Liu, H.-L. (2013). Influence of the El Niño Southern Oscillation on the middle and upper atmosphere. *Journal of Geophysical Research: Space Physics*, *118*, 2744–2755. https://doi.org/10.1002/jgra.50286

Pedatella, N. M., Liu, H.-L., Sassi, F., Lei, J., Chau, J. L., & Zhang, X. (2014). Ionosphere variability during the 2009 SSW: Influence of the lunar semidiurnal tide and mechanisms producing electron density variability. *Journal of Geophysical Research: Space Physics*, *119*, 3828–3843. https://doi.org/10.1002/2014JA019849

Pedatella, N. M., Oberheide, J., Sutton, E. K., Liu, H.-L., Anderson, J. L., & Raeder, K. (2016). Short-term nonmigrating tide variability in the mesosphere, thermosphere, and ionosphere. *Journal of Geophysical Research: Space Physics*, *121*, 3621–3633. https://doi.org/10.1002/2016JA022528

Rastogi, R. G., & Klobuchar, J. A. (1990). Ionospheric electron content within the equatorial F_2 layer anomaly belt. *Journal of Geophysical Research*, *95*(A11), 19,045–19,052. https://doi.org/10.1029/JA095iA11p19045

Rastogi, R. G., & Patil, A. (1986). Complex structure of equatorial electrojet current. *Current Science*, *55*(9), 433–436.

Richmond, A. D. (1995a). Modeling equatorial ionospheric electric fields. *Journal of Atmospheric and Solar-Terrestrial Physics*, *57*, 1103–1115.

Richmond, A. D. (1995b). Ionospheric electrodynamics. In H. Volland (Ed.), *Handbook of atmospheric electrodynamics* (Vol. 2, pp. 249–290). Boca Raton, Fla: CRC Press.

Richmond, A. D., Fang, T.-W., & Maute, andA. (2015). Electrodynamics of the equatorial evening ionosphere: 1. Importance of winds in different regions. *Journal of Geophysical Research: Space Physics*, *120*, 2118–2132. https://doi.org/10.1002/2014JA020934

Rush, C. M., & Richmond, A. D. (1973). The relationship between the structure of the equatorial anomaly and the strength of the equatorial electrojet. *Journal of Atmospheric and Terrestrial Physics*, *35*, 1171–1180.

Scherliess, L., & Fejer, B. G. (1999). Radar and satellite global equatorial *F* region vertical drift model. *Journal of Geophysical Research*, *104*(A4), 6829–6842. https://doi.org/10.1029/1999JA900025

Siddiqui, T. A., Stolle, C., Lühr, H., & Matzka, J. (2015). On the relationship between weakening of the northern polar vortex and the lunar tidal amplification in the equatorial electrojet. *Journal of Geophysical Research: Atmospheres*, *120*, 10,006–10,019. https://doi.org/10.1002/2015JA021683

Solomon, S. C., & Qian, L. (2005). Solar extreme-ultraviolet irradiance for general circulation models. *Journal of Geophysical Research*, *110*, A10306. https://doi.org/10.1029/2005JA011160

Stening, R. J. (1995). What drives the equatorial electrojet. *Journal of Atmospheric and Terrestrial Physics*, *57*, 1117–1128.

Stolle, C., Manoj, C., Lühr, H., Maus, S., & Alken, P. (2008). Estimating the daytime Equatorial Ionization Anomaly strength from electric field proxies. *Journal of Geophysical Research*, *113*, A09310. https://doi.org/10.1029/2007JA012781

Takeda, M. (1996). Effects of the strength of the geomagnetic main field strength on the dynamo action in the ionosphere. *Journal of Geophysical Research*, *101*(A4), 7875–7880. https://doi.org/10.1029/95JA03807

Tang, W., Xue, X.-H., Lei, J., & Dou, X.-K. (2014). Ionospheric quasi-biennial oscillation in global TEC observations. *Journal of Atmospheric and Solar-Terrestrial Physics*, *107*, 36–41.

Tao, C., Jin, H., Shinagawa, H., Fujiwara, H., & Miyoshi, Y. (2017). Effect of intrinsic magnetic field decrease on the low- to middle-latitude upper atmosphere dynamics simulated by GAIA. *Journal of Geophysical Research: Space Physics*, *122*, 9751–9762. https://doi.org/10.1002/2017JA024278

Tapping, K. F. (2013). The 10.7 cm solar radio flux ($F_{10.7}$). *Space Weather*, *11*, 394–406. https://doi.org/10.1002/swe.20064

Themens, D. R., Jayachandran, P. T., Galkin, I., & Hall, C. (2017). The Empirical Canadian High Arctic Ionospheric Model (E-CHAIM): N_mF_2 and h_mF_2. *Journal of Geophysical Research: Space Physics*, *122*, 9015–9031. https://doi.org/10.1002/2017JA024398

Uozumi, T., Yumoto, K., Kitamura, K., Abe, S., Kakinami, Y., Shinohara, M., et al. (2008). A new index to monitor temporal and long-term variations of the equatorial electrojet by MAGDAS/CPMN real-time data: *EE*-Index. *Earth, Planets and Space*, *58*, 1–11.

Vincent, R. A., Kovalam, S., Fritts, D. C., & Isler, J. R. (1998). Long-term MF radar observations of solar tides in the low-latitude mesosphere: Inter-annual variability and comparisons with the GSWM. *Journal of Geophysical Research*, *103*, 8667–8683. https://doi.org/10.1029/98JD00482

Woodman, R. F. (1970). Vertical velocities and east-west electric fields at the magnetic equator. *Journal of Geophysical Research*, *75*, 6249–6259.

Wu, Q., Ortland, D. A., Killeen, T. L., Roble, R. G., Hagan, M. E., Liu, H.-L., et al. (2008). Global distribution and interannual variations of mesospheric and lower thermospheric neutral wind diurnal tide: 1. Migrating tide. *Journal of Geophysical Research*, *113*, A05308. https://doi.org/10.1029/2007JA012542

Yamazaki, Y., & Kosch, M. J. (2015). The equatorial electrojet during geomagnetic storms and substorms. *Journal of Geophysical Research: Space Physics*, *120*, 2276–2287. https://doi.org/10.1002/2014JA020773

Yamazaki, Y., Liu, H., Sun, Y.-Y., Miyoshi, Y., Kosch, M. J., & Mlynczak, M. G. (2017). Quasi-biennial oscillation of the ionospheric wind dynamo. *Journal of Geophysical Research: Space Physics*, *122*, 3553–3569. https://doi.org/10.1002/2016JA023684

Yamazaki, Y., & Maute, A. (2017). Sq and EEJ—A review on the daily variation of the geomagnetic field caused by ionospheric dynamo currents. *Space Science Reviews*, *206*, 299–405. https://doi.org/10.1007/s11214-016-0282-z

Yamazaki, Y., & Richmond, A. D. (2013). A theory of ionospheric response to upward-propagating tides: Electrodynamic effects and tidal mixing effects. *Journal of Geophysical Research: Space Physics*, *118*, 5891–5905. https://doi.org/10.1002/jgra.50487

Yamazaki, Y., Richmond, A. D., Liu, H., Yumoto, K., & Tanaka, Y. (2012). Sq current system during stratospheric sudden warming events in 2006 and 2009. *Journal of Geophysical Research*, *117*, A12313. https://doi.org/10.1029/2012JA018116

Yamazaki, Y., Richmond, A. D., Maute, A., Liu, H.-L., Pedatella, N., & Sassi, F. (2014). On the day-to-day variation of the equatorial electrojet during quiet periods. *Journal of Geophysical Research: Space Physics*, *119*, 6966–6980. https://doi.org/10.1002/2014JA020243

Yamazaki, Y., Richmond, A. D., Maute, A., Wu, Q., Ortland, D. A., Yoshikawa, A., et al. (2014). Ground magnetic effects of the equatorial electrojet simulated by the TIE-GCM driven by TIMED satellite data. *Journal of Geophysical Research: Space Physics*, *119*, 3150–3161. https://doi.org/10.1002/2013JA019487

Yamazaki, Y., Yumoto, K., Cardinal, M. G., Fraser, B. J., Hattori, P., Kakinami, Y., & Yoshikawa, A. (2011). An empirical model of the quiet daily geomagnetic field variation. *Journal of Geophysical Research*, *116*, A10312. https://doi.org/10.1029/2011JA016487

Yiğit, E., & Medvedev, A. S. (2015). Internal wave coupling processes in Earth's atmosphere. *Advances in Space Research*, *55*, 983–1003.

Yizengaw, E., Moldwin, M. B., Zesta, E., Biouele, C. M., Damtie, B., Mebrahtu, A., et al. (2014). The longitudinal variability of equatorial electrojet and vertical drift velocity in the African and American sectors. *Annales de Geophysique*, *32*(3), 231–238. https://doi.org/10.5194/angeo-32-231-2014

Yizengaw, E., Zesta, E., Moldwin, M. B., Damtie, B., Mebrahtu, A., Valladares, C. E., & Pfaff, R. F. (2012). Longitudinal differences of ionospheric vertical density distribution and equatorial electrodynamics. *Journal of Geophysical Research*, *117*, A07312. https://doi.org/10.1029/2011JA017454

Yue, X., Schreiner, W. S., Lei, J., Rocken, C., Hunt, D. C., Kuo, Y.-H., & Wan, W. (2010). Global ionospheric response observed by COSMIC satellites during the January 2009 stratospheric sudden warming event. *Journal of Geophysical Research*, *115*, A00G09. https://doi.org/10.1029/2010JA015466

Zhao, B., Wan, W., Liu, L., & Ren, Z. (2009). Characteristics of the ionospheric total electron content of the equatorial ionization anomaly in the Asian–Australian region during 1996–2004. *Annales de Geophysique*, *27*, 3861–3873.

Zhou, Y.-L., Li, Wang, Xiong, C., Lühr, H., & Ma, S.-Y. (2016). The solar activity dependence of nonmigrating tides in electron density at low and middle latitudes observed by CHAMP and GRACE. *Annales de Geophysique*, *34*, 463–472.